

(Fig. 3A), several lakes show up as small, dark areas, whereas the same lakes appear as bright features in the October image (Fig. 3B). The change in signature indicates that the lakes may have drained over the period from September to October, causing the ice on the surface to collapse. The lake basins are regions of low correlation (16) in the October interferogram (Fig. 2C), indicating that they underwent substantial surface change during the 1-day period, such as would be caused by drainage-induced fracturing of the ice on the lake surface. This suggests that the probable drainage of the lakes was related in some way to the increase in velocity.

In the area near Jakobshavns Isbrae, several lakes periodically drain through large moulins (17). These moulins close off during the winter, when there is no meltwater input from the surface. After a lake forms in the summer, melting and water pressure reopen the moulin, allowing drainage. Some similar process, such as high basal water pressure opening or enlarging connections to the surface, may allow the lakes on the Ryder to drain near the end of the melt season. The increase in meltwater access to the bed might play a role in greater sliding velocity.

Alternatively, the increase in velocity could have opened crevasses, allowing the lakes to drain. In this case, lake drainage is an effect rather than a cause of the rapid flow, and the flow instability could be caused by changes in the basal water system alone. One possible scenario is that the presumed bedrock ridge causes ponding of subglacial water beneath the ice plain. This may take place if the upstream side of the bedrock ridge is 10 times steeper than the relatively low ice surface slope driving basal water downstream (18). Basal water pressure may increase to the point at which stable sliding is no longer possible and a mini-surge begins.

We do not know if mini-surges are common (perhaps seasonal) on the Ryder or other outlet glaciers. We also do not know if this is an indication of potential for a more profound flow instability, such as a surge, which could produce a substantial change in ice flux. Surging glaciers are known to shut down and restart (8). Perhaps what we observed on the Ryder was a surge that did not quite succeed.

REFERENCES AND NOTES

1. K. Echelmeyer and W. Harrison [*J. Glaciol.* **36**, 82 (1990)] looked for variation in the speed of Jakobshavns Isbrae, the fastest glacier in Greenland. Although they believed that there was a large seasonal input of meltwater to the bed, their measurements exhibited no significant seasonal variation.
2. R. M. Goldstein, H. Engelhardt, B. Kamb, R. M. Frolich, *Science* **262**, 1525 (1993).
3. I. Joughin, D. Winebrenner, M. Fahnestock, *Geophys. Res. Lett.* **22**, 571 (1995).
4. E. Rignot, K. Jezek, H. Sohn, *ibid.*, p. 575.
5. The term "mini-surge" was used by C. F. Raymond and S. Malone [*J. Glaciol.* **32**, 178 (1986)] and B. Kamb and H. Engelhardt [*ibid.* **33**, 27 (1987)] to describe pulses of high flow speed propagating down a valley glacier and related to basal water pressure. The event we observed occurred on a larger glacier, and we have no evidence for the propagation of a velocity pulse. The change in velocity was large and short-lived, thus matching several of the characteristics they observed. The Ryder speedup could be likened to a surge, but the event was too short to develop the changes in ice distribution characteristic of a surge.
6. J. G. Ferrigno *et al.*, *Ann. Glaciol.* **17**, 239 (1993).
7. M. Meier *et al.*, *J. Geophys. Res.* **99**, 15219 (1994).
8. B. Kamb *et al.*, *Science* **227**, 469 (1985).
9. Basin-wide accumulation was derived from data published by A. Ohmura and N. Reeh [*J. Glaciol.* **37**, 140 (1991)].
10. R. Goldstein, *Geophys. Res. Lett.* **22**, 2517 (1995).
11. Velocity differences below 150 m/year are accurate to within about 10 m/year. Where we measured larger differences, the errors may be greater because of proximity to regions where the phase could not be unwrapped (that is, have the modulo- 2π ambiguity removed).
12. Over large parts of the fast-moving areas, fringes remain visible but are too noisy to unwrap.
13. For equal flow rates, the pattern of fringes is three times denser for a 3-day versus a 1-day interferogram, because three times the displacement occurred. Where we could not estimate velocity, the noisy fringe patterns for the 1-day October interferogram were visually denser than for the 3-day interferogram (acquired March 1992 and representative of the normal flow mode), suggesting that the October 1995 speed is in excess of three times its normal rate over some of the faster moving area.
14. The effect of vertical displacement, which is proportional to horizontal speed, dominates the phase at length scales of less than a few kilometers (3). Thus, similar short-scale variation observed in the November and September interferograms indicates that the horizontal speeds are comparable.
15. B. Kamb *et al.*, *J. Geophys. Res.* **99**, 15231 (1994).
16. Temporal decorrelation is caused by shifts in the relative positions of subpixel scatterers between acquisition of the images, which can be caused by rapid ice motion or the collapse of lake ice.
17. H. Thomsen, L. Thorning, R. Braithwaite, *Geol. Surv. Greenland Nr.* **138** (1985).
18. W. S. B. Paterson, *The Physics of Glaciers* (Pergamon, Oxford, ed. 2, 1994).
19. M. Fahnestock, R. Bindschadler, R. Kwok, K. Jezek, *Science* **262**, 1530 (1993).
20. R. Kwok and M. Fahnestock, *IEEE Trans. Geosci. Remote Sensing* **34**, 189 (1996); I. Joughin, D. Winebrenner, M. Fahnestock, R. Kwok, W. Krabill, *J. Glaciol.* **42**, 10 (1996).
21. I. Joughin, R. Kwok, M. Fahnestock, *J. Glaciol.*, in press.
22. We thank B. Bindschadler and the reviewers for their comments on the manuscript, and C. Werner for providing the synthetic aperture radar processor. I.J. and R.K. performed this work at the Jet Propulsion Laboratory under contract with NASA. S.T. acknowledges support from the Henry and Grazyna Bauer fellowship. M.F. was supported under NASA Mission to Planet Earth grant NAGW4285. Radar data were supplied by the European Space Agency.

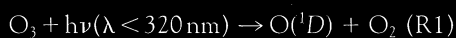
28 June 1996; accepted 21 August 1996

Observations of Near-Zero Ozone Concentrations Over the Convective Pacific: Effects on Air Chemistry

D. Kley,* P. J. Crutzen, H. G. J. Smit, H. Vömel, S. J. Oltmans, H. Grassl, V. Ramanathan

A series of measurements over the equatorial Pacific in March 1993 showed that the volume mixing ratios of ozone were frequently well below 10 nanomoles per mole both in the marine boundary layer (MBL) and between 10 kilometers and the tropopause. These latter unexpected results emphasize the enormous variability of tropical tropospheric ozone and hydroxyl concentrations, which determine the oxidizing efficiency of the troposphere. They also imply a convective short circuit of marine gaseous emissions, such as dimethyl sulfide, between the MBL and the uppermost troposphere, leading, for instance, to sulfate particle formation.

Because of the reactions



where h is Planck's constant, ν is frequency, and λ is wavelength, ozone (O_3) is the precursor molecule for hydroxyl (OH) radicals (1), the atmosphere's main oxidizing agent. The small fraction of atmospheric O_3 that is located in the troposphere thus plays a large role in the chemical composition of the atmosphere. In the stratosphere, photolysis of molecular oxygen (O_2) forms O_3 , of which a fraction is transported mostly to

the extratropical troposphere (2).

In the troposphere, reactions R1 + R2, and, in addition, reactions



are responsible for O_3 destruction (3). In the oceanic atmosphere, emissions of nitric oxide (NO) from the surface and lightning are small. With measured NO volume mix-

ing ratios in the low picomole per mole range, O₃ production is insignificant in the MBL and probably also above it (3, 4). Moreover, over the equatorial oceans, O₃ destruction by reactions R1 and R2 is strongly promoted by high levels of solar ultraviolet radiation and high humidity, resulting in a photochemical lifetime for O₃ of less than 1 week in the MBL (5). As a consequence, surface O₃ concentrations below 10 nmol/mol have been measured on various occasions over the tropical oceans (5–8). However, because of the strong exponential decrease of water vapor mixing ratios with altitude, O₃ lifetimes increase rapidly with height, to 1 month at 6 km and 1 year at 10 km. Therefore, above the MBL, O₃ may act as a tracer for convective transport. We report here a set of 25 O₃, water vapor, and temperature profile measurements over the tropical central Pacific obtained between 7 and 26 March 1993 (Fig. 1), which often show low O₃ concentrations both in the MBL and, most surprisingly, also in the upper troposphere (9).

The Central Equatorial Pacific Experiment (CEPEX) (10, 11) provided an opportunity to gather information on O₃ and water vapor concentrations in one of the Earth's most convective regions and its surroundings. Balloon-borne soundings were made from the ship *Vickers* between the Solomon Islands (9°24'S, 160°6'E) and Christmas Island (2°N, 157°30'W), mostly along 2°S. Satellite observations and meteorological analysis for the cruise gave evidence of widespread deep convective activity from 160°E to approximately the date-line (12). With some exceptions, convectively suppressed conditions prevailed thereafter during the cruise and subsequently over Christmas Island. We obtained profiles of temperature, pressure, and relative humidity every 6 hours for a total of 44 soundings, using radiosondes for the ship (13). Sixteen successful O₃ soundings were made from the ship and nine more from a location on Christmas Island (14).

The volume mixing ratios of O₃ in the MBL along the cruise track and those from

Christmas Island were consistently below 10 nmol/mol and on several occasions were below the detection limit of 3 to 5 nmol/mol (Fig. 1). Because of O₃ destruction in the MBL by reactions R1 through R5, surface O₃ mixing ratios are low in this region (5–8). The middle troposphere was characterized by somewhat higher, but still low,

mixing ratios. Extremely low O₃ mixing ratios of 0 to 10 nmol/mol were measured in the uppermost troposphere west of the date-line (profiles 1, 2, and 3) and on several occasions thereafter (profiles 5, 11, 14, and 16). Between the dateline and 173°W, mixing ratios were higher, but still relatively low (below 25 nmol/mol), in the upper

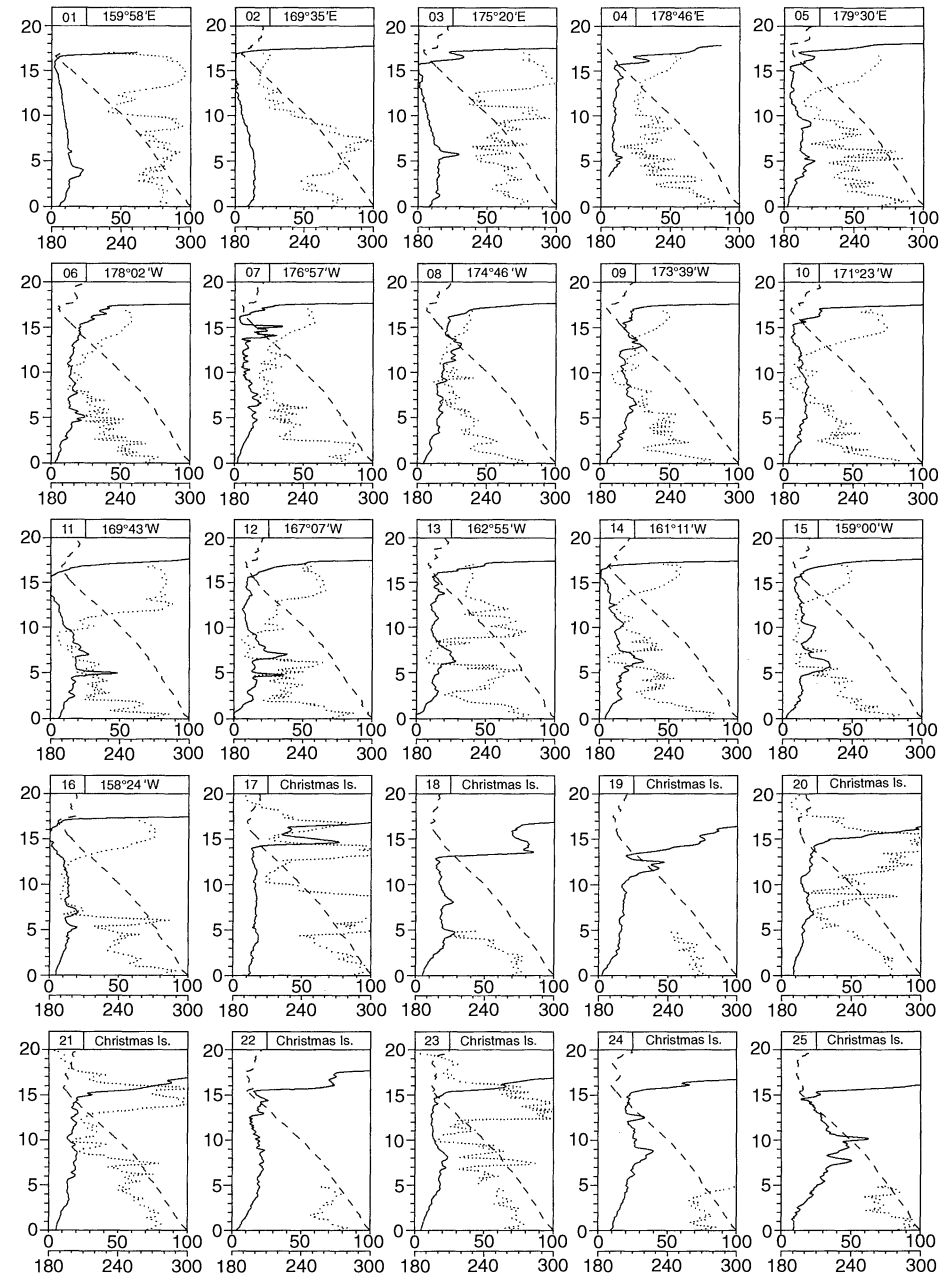


Fig. 1. Vertical profiles of temperature from 180 to 300 K (dashed lines), O₃ mixing ratio from 0 to 100 nmol/mol (solid lines), and relative humidity (0 to 100%) over water above 0°C and ice below 0°C (dotted lines) along the cruise track of the *Vickers*, 7 to 18 March 1993 (profiles 1 through 16), and over Christmas Island, 20 to 26 March 1993 (profiles 17 through 25). Temperature, relative humidity, and O₃ mixing ratio scales are given on the abscissa. The altitude, in kilometers, is given on the ordinate. The humidities for profiles 1 through 16 were measured with HUMICAP H sensors and those for soundings 18, 19, 22, 24, and 25 with HUMICAP A sensors. For profiles 17, 20, 21, and 23, frost-point hygrometers were used. Ozone and humidity measurements for profiles 17 through 25 were made simultaneously. Water and O₃ soundings for profiles 1 through 16 were made with a time delay of 2 ± 2 hours.

D. Kley and H. G. J. Smit, Institut für Chemie und Dynamik der Geosphäre, Forschungszentrum Jülich, 52425 Jülich, Germany.
 P. J. Crutzen, Max-Planck-Institut für Chemie, Postfach 3036, 55020 Mainz, Germany, and the Center for Clouds, Chemistry, and Climate, Scripps Institution of Oceanography, University of California at San Diego, La Jolla, CA 92093, USA.
 H. Vömel and S. J. Oltmans, Climate Monitoring and Diagnostics Laboratory, National Oceanic and Atmospheric Administration, Boulder, CO 80303, USA.
 H. Grassl, World Climate Research Programme, World Meteorological Organization, Geneva, Switzerland.
 V. Ramanathan, Center for Clouds, Chemistry, and Climate, Scripps Institution of Oceanography, University of California at San Diego, La Jolla, CA 92093, USA.

*To whom correspondence should be addressed.

troposphere (profiles 6 through 9).

During soundings 1 and 3, the troposphere was characterized by active deep convection to the tropopause. The low O₃ mixing ratios above 10 km were accompanied by relative humidity over ice exceeding 70% (Fig. 1). In fact, a relative humidity of 100% is possible within the uncertainty limits of the measurements (13, 15). An exception was sounding 2, where low O₃ mixing ratios in the upper troposphere coincided with low relative humidities (15).

The extremely low upper tropospheric O₃ mixing ratios suggest that convection had lifted low-level O₃-poor MBL air to the uppermost troposphere without significant entrainment between altitudes. Nevertheless, repeated observations of zero, or near-zero, O₃ in the upper troposphere at values below those in the MBL indicate that O₃ might be destroyed in clouds (16, 17). The low O₃ volume mixing ratios up to the tropopause and the extremely steep increase in the values above the tropopause in the convective situations indicate that the air flow was upward in the tropopause region, counteracting downward diffusion of O₃ from the stratosphere.

East of the dateline, the air was dry between 5 and 10 km, relative humidities were as low as 10%, and O₃ mixing ratios reached about 25 nmol/mol. During this part of the cruise, the troposphere was under conditions of suppressed convection (11). However, here three examples of extremely low O₃ volume mixing ratios were encountered near the tropopause, including several near-zero readings (soundings 11, 14, and 16). The meridional winds were from the south at speeds of 10 to 15 m/s for the air masses that showed the low O₃ values. The Geostationary Operational Environmental Satellite/Geostationary Meteorological Satellite (GOES/GMS) infrared images identified convective regions approximately 1 day upwind to the south of the locations where the O₃ and water vapor soundings were made (11). Therefore, those sampled air masses represent lateral outflows from regions with strong convection. It is thus likely that cases of low upper-tropospheric O₃ are the result of deep convection elsewhere as well.

Several soundings over the convectively suppressed region show comparatively high O₃ mixing ratios several kilometers below the tropopause. This result was especially pronounced for the Christmas Island profiles (soundings 17 through 25). Because the MBL O₃ mixing ratios are as small as those over the convective region, this suggests stratospheric influx as the source of the elevated tropospheric O₃ layers.

The low O₃ and NO concentrations and the strong reflection of solar radiation from

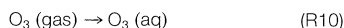
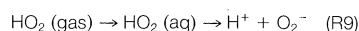
the anvil cloud deck lead to lower OH concentrations than elsewhere in the tropical troposphere. In the more convective parts of the marine tropics, this effect will result in reduced chemical removal rates of gases that are released to the atmosphere from the ocean. Box model calculations for a convective situation, based on a complete set of chemical measurements (7), indicate that the 12-hour average OH concentration was merely 5×10^5 molecules per cubic centimeter (18). This result implies that the photochemical lifetime of dimethyl sulfide (DMS) is 10 days, which exceeds the average boundary-layer evacuation time of about 5 to 10 days over the equatorial Pacific (19). Therefore, substantial amounts of this gas may escape oxidation in the MBL and reach the upper troposphere over convective regions. Thus, DMS may influence sulfate aerosol formation (20) in the upper troposphere and stratosphere. Observations of dimethyl sulfide [(CH₃)₂S] over the tropical Pacific have identified the presence of this short-lived compound in the MBL in mixing ratios from 50 to 500 pmol/mol (21). Another oceanic emission compound that may reach the upper troposphere is methyl iodide (CH₃I) (17), which after photodissociation may produce I and IO, possibly leading to catalytic O₃ destruction (17, 22).

Our data demonstrate the large variability of O₃ concentrations in the tropical troposphere. Concentrations can exceed 50 nmol/mol over the continents during the dry season (23, 24) and can approach zero levels in the MBL and in the upper troposphere in convective regions over the tropical Pacific. This result also implies that OH concentrations vary by an order of magnitude in the tropics and thus that there are major spatial and temporal fluctuations in the oxidizing efficiency of the atmosphere, which is largely determined by OH radicals in the tropical troposphere.

REFERENCES AND NOTES

1. H. Levy II, *Science* **173**, 141 (1971).
2. E. F. Danielsen and V. A. Mohnen, *J. Geophys. Res.* **82**, 5867 (1977).
3. If oxides of nitrogen were present in the troposphere in sufficient quantities, peroxy (RO₂) radicals, with R = H or CH₃, will react with NO (reaction R6), leading to O₃ production by
$$\text{RO}_2 + \text{NO} \rightarrow \text{OH} + \text{NO}_2 \quad (\text{R6})$$
$$\text{NO}_2 + h\nu(\lambda < 420 \text{ nm}) \rightarrow \text{NO} + \text{O} \quad (\text{R7})$$
$$\text{O} + \text{O}_2 + \text{M} \rightarrow \text{O}_3 + \text{M} \quad (\text{R8})$$
HO₂ is formed by reactions R3 and R4, and both HO₂ and CH₃O₂ are formed during the oxidation of methane (CH₄) [P. J. Crutzen, *Pure Appl. Geophys.* **106-108**, 1385 (1973); W. L. Chameides and J. C. G. Walker, *J. Geophys. Res.* **78**, 8751 (1973)].
4. M. McFarland, D. Kley, J. W. Drummond, A. L. Schmeltekopf, R. H. Winkler, *Geophys. Res. Lett.* **6**, 605 (1979); A. L. Torres and A. M. Thompson, *J. Geophys. Res.* **98**, 16949 (1993); W. L. Chameides *et al.*, *ibid.* **92**, 2131 (1987); C. Price and D. Rind, *Mon. Weather Rev.* **122**, 1930 (1994).

5. S. C. Liu, M. McFarland, D. Kley, O. Zafiriou, B. Huebert, *J. Geophys. Res.* **88**, 1360 (1983).
6. F. Routhier *et al.*, *ibid.* **85**, 7307 (1980); S. R. Pitotowicz, H. F. Bezdek, G. R. Harvey, M. Springer-Young, K. J. Hanson, *ibid.* **96**, 18679 (1991); J. E. Johnson *et al.*, *ibid.* **95**, 11847 (1990); S. J. Oltmans, *ibid.* **86**, 1174 (1981); _____ and W. D. Komhyr, *ibid.* **91**, 5229 (1986); H. B. Singh *et al.*, *ibid.* **101**, 1907 (1996).
7. A. M. Thompson *et al.*, *ibid.* **98**, 16955 (1993).
8. E. V. Browell *et al.*, *ibid.* **101**, 1691 (1996).
9. Ozone profiles obtained from aircraft measurements in the vicinity of the Intertropical Convergence Zone, south of Hawaii, have revealed low O₃ mixing ratios, near 12 nmol/mol, from the boundary layer to the ceiling altitude of the aircraft at 9 km [J. Fishman, G. L. Gregory, G. W. Sachse, S. M. Beck, G. F. Hill, *ibid.* **92**, 2083 (1987)]. Extensive lidar O₃ measurements were made over the equatorial western Pacific in September and October 1991, but extremely low O₃ mixing ratios in the upper troposphere were not recorded (8). Balloon soundings over the tropical Atlantic have shown that ascending air in the Hadley cell transports air with an O₃ mixing ratio near 30 nmol/mol from the low to the upper troposphere [H. G. J. Smit, S. Gilge, D. Kley, in *Physico-Chemical Behaviour of Atmospheric Pollutants*, G. Restelli and G. Angeletti, Eds. (Kluwer Academic, Dordrecht, Netherlands, 1990), pp. 630-637; R. Weller, R. Lili-schik, O. Schrems, R. Neuber, S. Wessel, *J. Geophys. Res.* **101**, 1387 (1996)].
10. *CEPEX Experiment Design Document* (Center for Clouds, Chemistry, and Climate, University of California, San Diego, CA, 1993).
11. *Central Equatorial Pacific Experiment (CEPEX): Daily Operations Summary* (prepared by S. F. Williams, University Cooperation for Atmospheric Research, Office of Field Project Support, Boulder, CO, 1993).
12. Composite GOES/GMS satellite infrared images are documented in (11). Cloud-top infrared brightness temperatures were obtained from the CEPEX Integrated Data System (accessible via <http://www-c4.ucsd.edu>).
13. Relative humidities for the ship soundings were determined with commercial capacitive sensors (HUMICAP H or A). The accuracy of the sensors above 5 km was assessed by occasional intercomparison of soundings, 2 to 4 hours apart, with balloon-borne frost-point hygrometers. The uncertainty of the humidity determination in the middle troposphere was $\pm 35\%$ over ice. In the uppermost layers of the troposphere, the uncertainty was $\pm 53\%$ (15).
14. Partial pressures of O₃ were measured by electrochemical O₃ sensors (ECC), which were flown together with radiosondes on small valved rubber balloons. The accuracy of the O₃ measurements was determined in a laboratory simulation chamber under quasi-flight conditions simulating pressure, temperature, and O₃. The accuracy of the O₃ partial pressure determination for CEPEX is 0.1 mPa. In terms of mixing ratios, the instrument accuracy was 1 to 2 nmol/mol below 5 km, increasing to ± 5 nmol/mol above 10 km [H. G. J. Smit, W. Sträter, D. Kley, M. H. Proffitt, in *Transport and Transformation of Pollutants in the Troposphere*, P. M. Borrell, P. Borrell, T. Cvitas, W. Seiler, Eds. (SPB Academic Publishing bv, Den Haag, Netherlands, 1994), pp. 349-353]. The O₃ partial pressure was measured during balloon ascent and descent. On descent through the upper troposphere, the ECC, after having been exposed to high stratospheric O₃ conditions, experienced some hysteresis, which renders the descent data from the upper troposphere (>5 km) of little use. Figure 1 gives mostly ascent data. A problem arises when reducing gases, such as sulfur dioxide (SO₂), interfere with the redox system of the ECC in conjunction with the sonde drifting through the ship's engine exhaust plume after balloon release. In such instances, data recorded during balloon descent were used for the first few hundred meters above the sea surface.
15. D. Kley *et al.*, in preparation.
16. Ozone destruction can take place as a result of dissolution and dissociation of HO₂ in cloud droplets or possibly on the surface of ice particles followed by reaction with O₃.



[J. Lelieveld and P. J. Crutzen, *Nature* **343**, 227 (1990); P. J. Crutzen, in *Composition, Chemistry, and Climate of the Atmosphere*, H. Singh, Ed. (Van Nostrand Reinhold, New York, 1995), pp. 349–393]. Because a significant Cl source has not been identified, Cl activation on the surface of ice particles, leading to O_3 loss, appears unlikely.

17. It has been proposed that reactions involving iodine radicals derived from CH_3I play a role in tropospheric O_3 destruction [D. D. Davis *et al.*, *J. Geophys. Res.* **101**, 2135 (1996)].
18. For the calculation of OH production rates we used the following parameters: water vapor mixing ratio = 18 g/kg (15); O_3 mixing ratios = 5 nmol/mol (Fig. 1); $\text{CO} = 75$ nmol/mol; and $\text{CH}_4 = 1.70$ $\mu\text{mol/mol}$ [T. J.

Bates, K. C. Kelly, J. E. Johnson, *J. Geophys. Res.* **98**, 16969 (1993)]. Measured diurnal values of the O_3 photodissociation coefficient [$J(\text{O}^1\text{D})$] for the formation of O^1D atoms according to reaction R1, under conditions of active convection in the Inter-tropical Convergence Zone of the Atlantic, were taken from A. Hofzumahaus, T. Brauers, U. Platt, and J. Callies [*J. Atmos. Chem.* **15**, 283 (1992)]. The 12-hour average was $J(\text{O}^1\text{D}) = 8.2 \times 10^{-6}$ per second. The total O_3 column densities were about 275 Dobson units for the Atlantic cruise and for CEPEX as well. Therefore, the Atlantic and the CEPEX relevant J values should be similar.

19. We calculated the boundary layer evacuation times for the CEPEX region using the National Center for Atmospheric Research CCM3 model (P. Rasch, personal communication) from monthly mean MBL air masses and the upward component of the deep convective mass fluxes.
20. C. A. Brock, P. Hamill, J. C. Wilson, H. H. Jonsson,

K. R. Chan, *Science* **270**, 1650 (1995).

21. M. O. Andreae *et al.*, *J. Geophys. Res.* **90**, 12891 (1985); S. A. Yvon, E. S. Saltzman, D. J. Cooper, T. S. Bates, A. M. Thompson, *ibid.* **101**, 6899 (1996); G. L. Gregory *et al.*, *ibid.*, p. 1727.
22. S. Solomon, R. R. Garcia, A. R. Ravishankara, *ibid.* **99**, 20491 (1994).
23. P. J. Crutzen and M. O. Andreae, *Science* **250**, 1669 (1990).
24. J. Fishman, K. Fakhruzzaman, B. Cros, D. Nganga, *ibid.* **252**, 1693 (1991).
25. We thank P. Rasch for supplying the estimates of the MBL evacuation times, and R. Vogt and J. Landgraf for carrying out the calculation on OH concentrations. This work was funded in part by NSF grant ATM 9405024. CEPEX was funded by NSF (ATM 8920119) and the Department of Energy (DE-F603-91ER61198).

29 May 1996; accepted 19 August 1996

Flow-Induced Molecular Orientation of a Langmuir Film

Takayuki Maruyama, Gerald Fuller,* Curtis Frank, Channing Robertson

The two-dimensional fluid dynamics of the different phases of a fatty acid monolayer (docosanoic acid) were examined. Brewster angle microscopy was used to investigate the polydomain structure of two "liquid condensed" phases (the L_2 and L'_2 phases) and the "solid" (S) phase in situ during an extensional flow. Only the L_2 phase deformed affinely with a liquid-like response. The two other phases experienced flow-induced reorientation of the lattice onto which the molecules were arranged. The reorientation process was accompanied by the appearance of shear bands in the monolayers at an angle of ± 45 degrees to the extension axis of the flow.

The flow behavior of monolayers at fluid-fluid interfaces is of fundamental and technological significance, and this subject has been reviewed at a micromechanical level by Edwards *et al.* (1). The influence of hydrodynamic forces on monolayers becomes apparent when their rheological responses are considered. These responses are often non-Newtonian, and shear-thinning surface viscosities are commonly encountered (2, 3), providing indirect evidence of flow-induced microstructural deformation and orientation within the layer. However, in most of the earlier work in surface rheology it has been assumed that the monolayers can sustain uniform flow fields. Moreover, the approaches have been predominantly concerned with macroscopic properties, such as the surface shear viscosity and modulus. The fact that most interfaces contain mesoscopic domain structures and orientatable molecules has often been neglected.

Measurements of flow-induced orientation at the molecular level have normally been performed on Langmuir-Blodgett films

where the material exposed to flow has been fixed to a solid substrate (4, 5). However, such an approach does not readily lend itself to the examination of transient phenomena, and the applied flow fields are usually inhomogeneous. Here, we used in situ measurements of molecular orientation at the fluid-fluid interface and used homogeneous flow fields with well-characterized velocity gradients.

The subject of this investigation was docosanoic acid, a fatty acid that has been extensively studied with respect to its equilibrium phase behavior when residing as a monolayer at the air-water interface. Pressure-area isotherms of Langmuir films reveal a number of phase transitions, and the corresponding structures have been examined by x-ray diffraction (6). The latter measurements revealed the existence of mesophases having positional order but not translational order. At the temperature used in this study (15°C), two distinct, first-order transitions were evident in pressure-area isotherms: one at a surface pressure of $\pi = 14.5$ mN m^{-1} and the other at $\pi = 27.5$ mN m^{-1} . The classical assignment of the first transition is between two "liquid condensed" phases, denoted as the L_2 and L'_2 phases, respectively. The second

transition separates the L'_2 phase from the S or "solid" phase. The L_2 phase has the head groups of the molecule on a distorted, hexagonal lattice with the alkyl chains' tails tilted at an angle toward their nearest lattice neighbor. As the monolayer is compressed, the tilt angle diminishes in magnitude, and across the transition the tilt direction switches toward the next nearest neighbor. As the monolayer enters the S phase, the tilt angle tends to zero and the alkyl chains are perfectly upright, but the head groups remain arranged on the distorted, hexagonal lattice.

The tilting of the alkyl tails of docosanoic acid makes Brewster angle microscopy (BAM) (7, 8) a convenient method with which to view the polydomain structure of this system. This optical probe uses light polarized in the plane of incidence that is reflected from the interface at the Brewster angle θ_B for the substrate (water, in the case of our Langmuir films). The presence of a thin film at the interface will cause the Brewster condition to be violated and light will be reflected. If the film consists of domains characterized by unique refractive indices, the reflected light will reveal the film morphology. The reflected light is viewed through an analyzing polarizer set to an angle α relative to the plane of incidence. An angle $\alpha = 60^\circ$ was found to optimize the contrast in the polydomain structure. To calculate the reflected light intensity, it is necessary to evaluate the matrix of reflection coefficients R_{ij} , (i, j) = p or s , where p and s refer to light polarized parallel and perpendicular to the plane of incidence, respectively. Of interest are the off-diagonal coefficients, R_{ps} and R_{sp} , which measure the tendency to convert p -polarized light to s polarization, and vice versa. The measured intensity is

$$I = I_0 [\cos^2 \alpha |R_{pp}|^2 + \sin^2 \alpha |R_{ss}|^2 + \cos \alpha \sin \alpha (R_{pp}R_{sp}^* + R_{pp}^*R_{sp})] \quad (1)$$

where I_0 is the incident light intensity and

Department of Chemical Engineering, Stanford University, Stanford, CA 94305-5025, USA.

*To whom correspondence should be addressed.